Performance and Analysis of Downlink Multiuser MIMO Systems With Regularized Zero-Forcing Precoding in Ricean Fading Channels

Harsh Tataria*, Peter J. Smith†, Larry J. Greenstein‡, Pawel A. Dmochowski*, Mansoor Shafi§
* School of Engineering and Computer Science, Victoria University of Wellington, Wellington, New Zealand
† School of Mathematics and Statistics, Victoria University of Wellington, New Zealand
‡ WINLAB, Rutgers University, North Brunswick, NJ, USA
§ Spark New Zealand, Wellington, New Zealand
email:{harsh.tataria, pawel.dmochowski}@ecs.vuw.ac.nz, peter.smith@vuw.ac.nz, ljg@winlab.rutgers.edu, mansoor.shafi@spark.co.nz

***Abstract*—Analytical expressions to approximate the expected per-user signal-to-interference-plus-noise-ratio (SINR) and ergodic sum-rate of a multiuser multiple-input-multiple-output system are presented. Our analysis assumes uncorrelated Ricean fading channels with regularized zero-forcing precoding on the downlink. The derived expressions are averaged with respect to the previously unknown arbitrary eigenvalue densities of the complex non-central Wishart distributed channel correlation matrix. To aid the derivation of the expected SINR, we derive analytical expressions for the joint density of two arbitrary eigenvalues of the complex non-central Wishart matrix. Unlike previous studies, our model caters to the presence of a unique Rice factor for each user terminal, making it suitable for analysis of modern systems, such as small cells and millimeter-wave. Our findings suggest that while the presence of strong line-of-sight has an adverse effect on the expected SINR and ergodic sum-rates, increasing the variability of Rice factors enhances the peak rate performance of the system. Our analysis can be applied to arbitrary system dimensions and is seen to remain tight across the signal-to-noise-ratio range considered.**

I. Introduction

Multiuser multiple-input-multiple-output (MU-MIMO) systems have received considerable attention in recent times due to their multiplexing gains and their ability to jointly serve a multiplicity of user terminals over the same time-frequency interval [1]. On the downlink, this has led to enhancements in the spectral efficiency and bit error rate [2]. Due to the broadcast nature of the downlink channel, MU-MIMO systems typically suffer from inter-user interference, leading to lower per-user signal-to-interference-plus-noise-ratio (SINR) and spectral efficiency. This has greatly motivated the use of channel aware pre-processing techniques, such as spatial precoding at the base station (BS). With channel knowledge at the BS, high complexity, non-linear precoding techniques such as dirty-paper coding (DPC) are known to achieve capacity [3]. In comparison, sub-optimal, linear pre-processing techniques have been identified as more practical due to their lower complexity [4].

More recently, with the focus on large antenna arrays at the BS, for measured non-line-of-sight (NLoS) channels, linear pre-processing techniques such as zero-forcing precoding have achieved 98% of DPC capacity [5]. However, to overcome noise inflation in the low signal-to-noise-ratio (SNR) regime, regularized zero-forcing (RZF) precoding was proposed in [4]. Several works have theoretically characterized the SINR and spectral efficiency gains of downlink MU-MIMO systems with RZF pre-processing (see [4, 6] and references therein). However, most works tend to adopt the simple Rayleigh fading model, appropriate for modeling rich scattering environments. Rayleigh fading fails to capture the presence of line-of-sight (LoS), which may be a dominant feature of future wireless systems operating with large antenna arrays in small cells, using the candidate millimeter-wave (mmWave) spectrum [7]. Thus, understanding the performance of MU-MIMO systems operating with LoS conditions is of growing importance. Limited numbers of works have considered the use of Ricean fading channels in the MU-MIMO context [8–10], where the focus has largely been on analyzing sum-rate and energy efficiency performance of the system, rather than performance on a per-user basis. Moreover, for simplicity, [8–10] evaluate the system performance with a fixed Rice factor for each terminal, despite their different geographical locations.

Unlike [8–10], in this paper, we consider a Ricean fading channel model, where we examine the effects of LoS propagation on the expected per-user SINR and ergodic sum-rate of a downlink MU-MIMO system with RZF precoding. We consider both microwave and mmWave channel parameters, where we develop a general analysis methodology scalable to any system dimension and SNR levels. To the best of authors' knowledge, such general treatment of the expected per-terminal and ergodic sum-rate analysis has not been carried out previously. Moreover, we analyze the per-user and system performance with a unique Rice factor for each terminal. More specifically, our main contributions can be summarized as follows:

- We derive tight analytical expressions to approximate the expected per-user SINR and ergodic sum-rate of the system with Ricean fading channels. Expected signal and interference powers are derived by averaging over the appropriate eigenvalue densities of the complex non-central Wishart channel correlation matrix. To the best of

the authors' knowledge, such an analysis has not been carried out previously.
- To aid the derivation of the expected per-user SINR, we derive analytical expressions for the joint density of a pair of arbitrary eigenvalues of the non-central Wishart distribution. This too has not been studied previously, with prior works targeting approximations to mimic the non-central Wishart structure (see [8, 9]).
- Our analysis is robust to changes in system dimension and considers the important case where each user in the system has a unique Rice factor. Our findings suggest that increasing the mean of the Rice factor in both the microwave and mmWave frequency bands has an adverse effect on the expected per-user SINR and ergodic sum-rate. Moreover, with a fixed mean, we demonstrate the impact of increased Rice factor variability, where we show that the onset of low Rice factors results in a larger occurrence of higher rates.

Notation: Boldface lower and upper case symbols represent vectors and matrices, respectively. $\boldsymbol{I}_M$ is the $M \times M$ identity matrix and diag $(\boldsymbol{H})$ denotes diagonal entries of $\boldsymbol{H}$. The transpose, Hermitian transpose and inverse operators are denoted by $(\cdot)^{\mathrm{T}}$, $(\cdot)^{\mathrm{H}}$ and $(\cdot)^{-1}$, respectively. We use $\boldsymbol{h} \sim \mathcal{CN}\left(\mu, \sigma^2\right)$ to denote a complex Gaussian distribution for $\boldsymbol{h}$, where each element of $\boldsymbol{h}$ has mean μ and variance σ^2. $||\cdot||_{\mathrm{F}}$ and $|\cdot|$ denote the Frobenius and scalar norms, while $\forall$ reads as "for all". $\mathbb{E}[\cdot]$, per $(\cdot)$ and $\lfloor\cdot\rfloor$ represent statistical expectation, permutation and floor operators, respectively.

II. System Model

We consider the downlink of a single cell, MU-MIMO system in an urban microcell (UMi) environment. The BS is equipped with M transmit antennas configured in a uniform linear array (ULA) to serve L non-cooperative single antenna user terminals ($M \geq L$) in the same time-frequency interval.

A. Channel Model

We assume an uncorrelated Ricean fading channel where the $1 \times M$ small-scale fading channel between the BS and the l-th user terminal can be expressed as

$$\boldsymbol{h}_l = \sqrt{\frac{K_l}{K_l+1}}\bar{\boldsymbol{h}}_l + \sqrt{\frac{1}{K_l+1}}\boldsymbol{h}_{w,l}. \tag{1}$$

The specular (LoS) and diffuse (scattered) components of the channel are denoted by $\bar{\boldsymbol{h}}_l$ and $\boldsymbol{h}_{w,l}$, respectively. K_l is the unique Rice (K) factor for the l-th user terminal, denoting the ratio between the power of the specular and diffuse components [11]. $\boldsymbol{h}_{w,l} \sim \mathcal{CN}(0,1)$, while the specular component of the channel is governed by the response of its transmit array steering vector, $\bar{\boldsymbol{h}}_l = [1, e^{j2\pi d\cos(\theta_l)}, \ldots, e^{j2\pi d(M-1)\cos(\theta_l)}]$ [12]. Here, d is the equidistant antenna spacing normalized by the carrier wavelength and θ_l is the angle-of-departure (AoD) of the specular component, for the l-th user terminal. As we consider uncorrelated downlink transmission, we set the inter-element spacing to a half-wavelength and assume that θ_l is uniformly distributed within the interval $[0, 2\pi]$. From the definition of the per-user channel in (1), a composite $L \times M$ small-scale fading channel matrix $\tilde{\boldsymbol{H}} \triangleq \left[\boldsymbol{h}_1^{\mathrm{T}}, \boldsymbol{h}_2^{\mathrm{T}}, \ldots, \boldsymbol{h}_L^{\mathrm{T}}\right]^{\mathrm{T}}$. This can also be written as

$$\tilde{\boldsymbol{H}} = \sqrt{\boldsymbol{\Phi}}\left(\sqrt{\bar{K}}\bar{\boldsymbol{H}} + \boldsymbol{H}_w\right) = \sqrt{\boldsymbol{\Phi}}\boldsymbol{H}, \tag{2}$$

where $\bar{K} \triangleq (1/L)\sum_{l=1}^{L} K_l$, $\boldsymbol{\Phi} \triangleq \mathrm{diag}\left(\frac{1}{K_1+1}, \ldots, \frac{1}{K_L+1}\right)$, the composite specular channel matrix $\bar{\boldsymbol{H}} \triangleq \left[\sqrt{\frac{K_1}{\bar{K}}}\bar{\boldsymbol{h}}_1^{\mathrm{T}}, \ldots, \sqrt{\frac{K_L}{\bar{K}}}\bar{\boldsymbol{h}}_l^{\mathrm{T}}\right]^{\mathrm{T}}$ and $\boldsymbol{H}_w$ is the composite diffuse channel matrix, respectively. We model the distribution of user terminals in the cell as uniform with respect to (w.r.t.) the cell area. The received power at the l-th terminal is denoted by $\tilde{\beta}_l = \rho A \zeta_l (r_0/r_l)^{\alpha}$ and is composed of the total transmit power, ρ, with large-scale fading effects. In particular, A is the unit-less constant for the geometric attenuation at a reference distance r_0, r_l is the link distance between the BS and the l-th terminal, α is the attenuation exponent and ζ_l represents the effects of shadow fading which follows a log-normal distribution, i.e., $10\log_{10}\zeta_l \sim \mathcal{N}\left(0, \sigma_{\mathrm{sh}}^2\right)$. Since $\boldsymbol{\Phi}$ simply scales the user channels, the *overall* channel can be viewed as a small-scale fading channel matrix, $\boldsymbol{H}$, with equivalent received powers, $\beta_l = \boldsymbol{\Phi}_{l,l}\tilde{\beta}_l = \tilde{\beta}_l (K_l+1)^{-1}$. This *overall* channel is used throughout the paper, which allows us to leverage previous analytical results on Ricean channels of the form in (2). For the remainder of the paper, we refer to SNR as the ratio of the long term received signal power to the noise power at the receiver.

Conditioned on the cell size and the relative proximity of the user terminals to the BS, we employ a probability based approach following [13, 14] to statistically determine if a given terminal experiences LoS or NLoS propagation conditions. The LoS and NLoS probabilities are a function of the link distance, from which the LoS and NLoS geometric attenuation and other link characteristics are obtained. We consider transmission in both the microwave and mmWave frequency bands for which we employ propagation parameters from [13] for the former and [14] for the latter. We delay the discussion of the above mentioned parameters to Section IV.

B. Per-User SINR and Ergodic Sum-Rate

We assume narrow-band transmission with equal power allocation to each user terminal. With perfect channel knowledge at the BS, the received signal at the l-th user terminal can be written as

$$y_l = \sqrt{\frac{\beta_l}{\eta}}\boldsymbol{h}_l\boldsymbol{w}_l s_l + \sqrt{\frac{\beta_l}{\eta}}\sum_{\substack{i=1\\ i\neq l}}^{L}\boldsymbol{h}_l\boldsymbol{w}_i s_i + z_l, \tag{3}$$

where $\boldsymbol{w}_l$ is the un-normalized precoding vector from the BS to terminal l, s_l is the data symbol desired for terminal l, such that $\mathbb{E}\left[|s_k|^2\right] = 1$. η is the precoder normalization to ensure that the overall transmit power remains unchanged. $z_l \sim \mathcal{CN}\left(0, \sigma_l^2\right)$ models the effects of additive white Gaussian noise at l-th terminal. In this paper, we consider RZF precoding to design the downlink precoding vectors, where $\boldsymbol{w}_l$ is the l-th column of the $M \times L$ precoding matrix, $\boldsymbol{W}$, defined as

$$\boldsymbol{W} \triangleq \left(\boldsymbol{H}^{\mathrm{H}}\boldsymbol{H} + \xi\boldsymbol{I}_M\right)^{-1}\boldsymbol{H}^{\mathrm{H}}. \tag{4}$$

Here $\xi = L/\text{SNR} \geq 0$ denotes the regularization parameter chosen from [4] to maximize SINR at the terminal. Following [15], the RZF precoding matrix is normalized with $\eta = ||\boldsymbol{W}||_{\text{F}}^2/L$, ensuring the total transmit power remains ρ. The received signal in (3) can be translated into a received SINR and expressed as

$$\text{SINR}_l = \frac{\frac{\beta_l}{\eta}|\boldsymbol{h}_l\boldsymbol{w}_l|^2}{\sigma_l^2 + \frac{\beta_l}{\eta}\sum\limits_{\substack{i=1\\ i\neq l}}^{L}|\boldsymbol{h}_l\boldsymbol{w}_i|^2}. \tag{5}$$

To this end, the instantaneous achievable downlink rate of the l-th user can be computed as $\text{R}_l = \log_2(1+\text{SINR}_l)$. As such, the ergodic sum-rate (measurable in bits/seconds/Hz) is

$$\mathbb{E}[\text{R}_{\text{sum}}] = \mathbb{E}\left[\sum_{l=1}^{L}\log_2(1+\text{SINR}_l)\right], \tag{6}$$

where the expectation is taken over the small-scale fading in $\boldsymbol{H}$. For the remainder of the paper, we denote $m = \min(M,L)$ and $n = \max(M,L)$, assuming $M \geq L$, as mentioned earlier. In the following section, we derive tight analytical expressions to approximate the expected per-user SINR and ergodic sum-rate of the system.

III. Expected SINR and Ergodic Sum-Rate Approximations

The expected per-user SINR at the l-th user terminal can be approximated as [16]

$$\mathbb{E}[\text{SINR}_l] \approx \frac{\frac{\beta_l}{\tilde{\eta}}\mathbb{E}\left[|\boldsymbol{h}_l\boldsymbol{w}_l|^2\right]}{\sigma_l^2 + \frac{\beta_l}{\tilde{\eta}}\sum\limits_{\substack{i=1\\ i\neq l}}^{L}\mathbb{E}\left[|\boldsymbol{h}_l\boldsymbol{w}_i|^2\right]}, \tag{7}$$

where $\tilde{\eta} = \mathbb{E}[\eta]$. In the following, we derive the expectations in (7) for the respective signal and interference powers.

A. Expected Signal Power

Via an eigenvalue decomposition, we denote $\boldsymbol{H}^{\text{H}}\boldsymbol{H} = \boldsymbol{Q}\boldsymbol{\Lambda}\boldsymbol{Q}^{\text{H}}$. Then, from [4], the expected value of the desired signal power in (7) can be written as

$$\delta_l = \mathbb{E}\left[|\boldsymbol{h}_l\boldsymbol{w}_l|^2\right] = \mathbb{E}\left[\left(\sum_{i=1}^{m}\frac{\lambda_i}{\lambda_i+\xi}|q_{l,i}|^2\right)^2\right]. \tag{8}$$

Here, λ_i is the i-th eigenvalue corresponding to the i-th diagonal entry in $\boldsymbol{\Lambda}$ and $q_{l,i}$ denotes the entry of $\boldsymbol{Q}$ corresponding to row l and column i, respectively. Further taking the expectation over the entries of $\boldsymbol{Q}$ yields [4]

$$\delta_l = \frac{1}{m(m+1)}\left\{\mathbb{E}\left[\left(\sum_{i=1}^{m}\frac{\lambda_i}{\lambda_i+\xi}\right)^2\right] + \mathbb{E}\left[\sum_{i=1}^{m}\left(\frac{\lambda_i}{\lambda_i+\xi}\right)^2\right]\right\}. \tag{9}$$

Note that (9) relies on an isotropic distribution for $\boldsymbol{Q}$, which does not hold for a fixed specular component. However, if averaged over the random AoD values in the transmit array steering response, $\boldsymbol{Q}$ retains its isotropic properties leading to (9). The expectations in (9) can be evaluated further over the eigenvalue densities of $\boldsymbol{H}^{\text{H}}\boldsymbol{H}$ and are presented in Theorems 1 and 3, respectively.

Theorem 1: Let $\phi_1,\ldots,\phi_m$ be the m eigenvalues of $\bar{K}\bar{\boldsymbol{H}}^{\text{H}}\bar{\boldsymbol{H}}$, then the expected value of $\sum_{i=1}^{m}\frac{(\lambda_i)^c}{(\lambda_i+\xi)^2}$ w.r.t. the eigenvalues of $\boldsymbol{H}^{\text{H}}\boldsymbol{H}$, an uncorrelated non-central Wishart matrix, is given by

$$G_l^{(c)} = m\left[\Theta\sum_{j=1}^{m}\sum_{\substack{i=1\\ i\neq j}}^{m}\sum_{p=0}^{\infty}\frac{\left(\bar{K}+1\right)^{n-m+j}\left(\left(\bar{K}+1\right)\phi_i\right)^p\mathcal{D}(i,j)}{p!(n-m+1)_p}\right.$$
$$\left.\sum_{\gamma=0}^{\bar{\mu}}\binom{\bar{\mu}}{\gamma}(-\xi)^{\bar{\mu}-\gamma}e^{\xi\left(\bar{K}+1\right)}\int_{\xi}^{\infty}x^{\gamma-2}e^{-x\left(\bar{K}+1\right)}dx\right]. \tag{10}$$

Here, $\bar{\mu} = c-1+n-m+j$,

$$\Theta = \frac{e^{-\sum_i\phi_i}}{m\left((n-m)!\right)^m\prod\limits_{k<q}^{m}(\phi_q-\phi_k)} \tag{11}$$

and $\mathcal{D}(i,j)$ is the (i,j)-co-factor of the $m\times m$ matrix $\boldsymbol{A}$, whose (q,k)-th entry is given by $(\boldsymbol{A})_{q,k} = (n-m+k-1)!\,{}_1F_1(n-m+k, n-m+1, \phi_q)$, with ${}_1F_1$ being a Kummer confluent hypergeometric function. Moreover, $(n-m+1)_p = (n-m+p)!/(n-m)!$ and

$$\int_{\xi}^{\infty}x^{\gamma-2}e^{-x\left(\bar{K}+1\right)}dx = \Psi\times\begin{cases}-\text{Ei}(1,\tilde{\xi}) + \frac{e^{-\tilde{\xi}}}{\tilde{\xi}^2} & ;\gamma=0\\ \text{Ei}(1,\tilde{\xi}) & ;\gamma=1\\ \Gamma(\gamma-1,\tilde{\xi}) & ;\gamma\geq 2,\end{cases} \tag{12}$$

where $\Psi = \frac{1}{\left(\bar{K}+1\right)^{\gamma-1}}$, $\tilde{\xi} = \xi\left(\bar{K}+1\right)$, $\text{Ei}(\cdot,\cdot)$ is the generalized exponential integral and $\Gamma(\cdot,\cdot)$ is the incomplete gamma function, respectively.

Proof: See Appendix A.

Theorem 2: With $\phi_1,\ldots,\phi_m$ as the m eigenvalues of $\bar{K}\bar{\boldsymbol{H}}^{\text{H}}\bar{\boldsymbol{H}}$, the joint density of any two arbitrary eigenvalues, (λ_1,λ_2), of $\boldsymbol{H}^{\text{H}}\boldsymbol{H}$ is given by

$$f(\lambda_1,\lambda_2) = C\sum_{i=0}^{m-1}\sum_{\substack{j=0\\ j\neq i}}^{m-1}\sum_{r=1}^{m}\sum_{\substack{s=1\\ s\neq r}}^{m}(-1)^u\,\tilde{\boldsymbol{\Xi}}(r,s;i,j)\,g_{r,i}(\lambda_1)\,g_{s,j}(\lambda_2), \tag{13}$$

where $u = i+j+r+s-p(i,j)-t(r,s)$ with

$$p(i,j) = \begin{cases}0 & ;j\leq i\\ 1 & ;j>i\end{cases}\text{ and }t(r,s) = \begin{cases}0 & ;s\leq r\\ 1 & ;s>r.\end{cases} \tag{14}$$

$$C = \Theta\left[(\varsigma-1)!\right]^m(-1)^{\lfloor\frac{m}{2}\rfloor}(n-2)!, \tag{15}$$

where Θ is as defined in (11). $\varsigma = n-m+1$,

$$\tilde{\boldsymbol{\Xi}}(r,s;i,j) = (\phi_r\phi_s)^{-v/2}\,\boldsymbol{\Xi}(r,s;i,j) \tag{16}$$

and $g_{a,b}(\lambda) = \lambda^{v/2+b}e^{-\lambda}\text{I}_v\left(2\sqrt{\phi_a\lambda}\right)$, where $v = n-m$. $\boldsymbol{\Xi}(r,s;i,j)$ is a determinant with rows r, s and columns i, j removed, where the d-th entry of the f-th column is given by $\frac{\Gamma(\varsigma+\varrho_f)}{\Gamma(\varsigma)}\,{}_1F_1(\varsigma+\varrho_f,\varsigma,\phi_d)$. $\varrho_f = f-1$, $\Gamma(\cdot)$ is the gamma function and $\text{I}_v(\cdot)$ is the modified Bessel function of the first kind.

Proof: See Appendix B.

Remark 1: Theorem 2 is used in computing the expected

per-user SINR and has general applicability for analysis involving complex non-central Wishart matrices. Prior works (see [8, 9]) often approximate the non-centrality of the Wishart matrix by its central counterpart via an adjustment of its covariance matrix. In contrast with this, we analyze the non-central Wishart structure in its exact form for further analysis in Theorem 3.

Theorem 3: With $\phi_1, \ldots, \phi_m$ as the m eigenvalues of $\bar{K}\bar{\boldsymbol{H}}^{\mathrm{H}}\bar{\boldsymbol{H}}$, the expected value of $\left(\sum_{i=1}^{m} \frac{\lambda_i}{\lambda_i+\xi}\right)^2$ w.r.t. the eigenvalues of $\boldsymbol{H}^{\mathrm{H}}\boldsymbol{H}$ is given by

$$D_l = G_l^{(2)} + \mathbb{E}_\lambda\left[\sum_{a=1}^{m}\sum_{\substack{b=1\\b\neq a}}^{m}\left(\frac{\lambda_a}{\lambda_a+\xi}\right)\left(\frac{\lambda_b}{\lambda_b+\xi}\right)\right] = G_l^{(2)} + m(m-1)\,C\sum_{i=0}^{m-1}\sum_{\substack{j=0\\j\neq i}}^{m-1}\sum_{r=1}^{m}\sum_{\substack{s=1\\s\neq r}}^{m}(-1)^u\,\Delta, \quad (17)$$

where C and u are as defined in (15) and (13), respectively. $\Delta = \tilde{\boldsymbol{\Xi}}(r,s;i,j)\,J_{r,i}J_{s,j}$, where $\tilde{\boldsymbol{\Xi}}(r,s;i,j)$ is as defined in (16) and

$$J_{a,b} = \sum_{\varepsilon=0}^{\infty}\left[\frac{\phi_a^{\varepsilon+\frac{n-m}{2}}}{\varepsilon!\,(\varepsilon+n-m)!}\right]\sum_{\gamma=0}^{\hat{\mu}}\binom{\hat{\mu}}{\gamma}(-\xi)^{\hat{\mu}-\gamma}e^{\xi}\int_{\xi}^{\infty}x^{\gamma-1}e^{-x}dx, \quad (18)$$

where $\hat{\mu} = \varepsilon + n - m + b + 1 \geq 2$ and the integral in (18) is a special case of the integral in (12).

Proof: See Appendix C.

Using the derived results in (10) and (17), the expected signal power at the l-th user terminal in (9) can be written as

$$\delta_l = \frac{D_l + G_l^{(2)}}{m\,(m+1)}. \quad (19)$$

The expected value of the precoder normalization parameter can also be found from the derived results such that

$$\tilde{\eta} = \frac{1}{m}\mathbb{E}\left[||\boldsymbol{W}||_{\mathrm{F}}^2\right] = \frac{1}{m}\mathbb{E}_\lambda\left[\sum_{i=1}^{m}\frac{\lambda_i}{(\lambda_i+\xi)^2}\right] = \frac{G_l^{(1)}}{m}. \quad (20)$$

B. Expected Interference Power

The total expected received power (desired and interfering powers) at the l-th terminal can be written as [4]

$$\varphi_l = \frac{\mathbb{E}\left[||\boldsymbol{H}\boldsymbol{W}||_{\mathrm{F}}^2\right]}{m} = \frac{1}{m}\left[\mathbb{E}_\lambda\left\{\sum_{i=1}^{m}\left(\frac{\lambda_i}{\lambda_i+\xi}\right)^2\right\}\right] = \frac{G_l^{(2)}}{m}. \quad (21)$$

Following [4], we define the expected interference power at user l, ι_l, as the difference between the total expected received power and the expected signal power. Thus,

$$\iota_l = \varphi_l - \delta_l = \frac{G_l^{(2)}}{m} - \frac{D_l + G_l^{(2)}}{m\,(m+1)}. \quad (22)$$

Using (19), (20) and (22), the expected SINR for the l-th terminal can now be written as a function of δ_l and $\tilde{\eta}$ and ι_l as

$$\mathbb{E}\left[\mathrm{SINR}_l\right] \approx \frac{\frac{\beta_l}{\tilde{\eta}}\delta_l}{\sigma_l^2 + \frac{\beta_l}{\tilde{\eta}}(m-1)\,\iota_l}. \quad (23)$$

Remark 2: The generality of the results derived in Theorems 1 and 3 is worth mentioning. The theorems are applicable for any system dimension and hold for arbitrary rank LoS and NLoS channels [17]. The derived results can also be applied to other systems, such as small cell networks, where a hierarchy of BSs may be present. In such cases, the additional presence of inter-cellular interference can be characterized in exactly the same manner as above [18].

Using Jensen's inequality, the approximated per-user SINR in (23) can be translated into an upper bound on the ergodic sum-rate, written as [3]

$$\mathbb{E}\left[\mathrm{R}_{\mathrm{sum}}\right] \leq \sum_{l=1}^{L}\log_2\left(1+\mathbb{E}\left[\mathrm{SINR}_l\right]\right), \quad (24)$$

where the expectation is again taken over the fast-fading in $\boldsymbol{H}$. The accuracy of the derived analytical expressions is demonstrated in the following section.

IV. Numerical Results

In this section, we present numerical results for a UMi scenario with the parameters specified in Table I. Unless otherwise specified, parameters for the microwave and mmWave cases were selected from [13] and [14], respectively. Based on the link distance, r_l, we employ a probabilistic approach to determine whether the user terminal experiences LoS or NLoS conditions. For the microwave case, the probability of the l-th user terminal experiencing LoS is governed by [13]

Parameter	Value	
	Microwave	**mmWave**
Carrier frequency [GHz]	2	28
Transmit power $[\rho]$ [dBm]	30	30
Bandwidth [MHz]	20	100
Noise variance [dBm]	-120	-113
LoS attenuation exponent $[\alpha]$	2.2	2
NLoS attenuation exponent	3.67	2.92
LoS unit-less attenuation constant $[A]$ [dB]	28	61.4
NLoS unit-less attenuation constant	22.7	72
LoS shadow fading standard deviation $[\sigma_{\mathrm{sh}}]$	3	5.8
NLoS shadow fading standard deviation	4	8.7
K-Factor mean [dB]	9	12 [19]
K-Factor standard deviation [dB]	5	3 [19]

TABLE I
System Parameters

$$P_{\mathrm{LoS}}(r_l) = \left(\min\left(18/r_l, 1\right)\left(1-e^{-r_l/36}\right)\right) + e^{-r_l/36}. \quad (25)$$

Naturally, the probability of the user experiencing NLoS is then determined by $P_{\mathrm{NLoS}} = 1 - P_{\mathrm{LoS}}$. Equivalently, for the mmWave case [14],

$$P_{\mathrm{LoS}}(r_l) = \left(1 - P_{\mathrm{out}}(r_l)\right)e^{-\omega_{\mathrm{LoS}}\,r_l}, \quad (26)$$

where $1/\omega_{\mathrm{LoS}} = 67.1$ meters and P_{out} is the outage probability, occurring when the attenuation in either the LoS or NLoS states is sufficiently large. For simplicity, in this study we set $P_{\mathrm{out}} = 0$ in determining the LoS and NLoS probabilities. Note that (26) is also applicable for performance evaluation at frequencies higher than 28 GHz, such as 73 GHz as shown

in [14]. Upon determining the link state of each terminal, we select the corresponding link parameters to model the large-scale propagation effects of geometric attenuation and shadow fading, as specified in Table I. Following [13] and [19], we assign a unique K-factor, K_l, for the l-th user terminal from a log-normal distribution with the mean and standard deviation specified in Table I. We refer to this as $K \sim \ln(\text{mean}, \text{standard deviation})$. It is worth observing that the mean of K increases, while its standard deviation decreases, as we transition from microwave to mmWave frequency bands.

First, the accuracy of the proposed expected per-user SINR in (23) is examined. Fig. 1 illustrates the expected SINR for a given terminal as a function of SNR for a system with $M = 10$ and $L = 3$. In addition to the microwave and mmWave cases, we consider uncorrelated Rayleigh fading as a baseline case for comparison purposes. Also for comparison purposes, we consider the case where each user terminal is assigned a fixed K-factor of 5 dB. Two trends can be observed: First is the fact that increasing the mean of K has an adverse effect on the expected SINR. This is due to the fact that an increase in the mean K implies a stronger specular component in the channel, which reduces multi-path diversity and in turn reduces the channel rank. Equivalently, this effect can be interpreted by an increase in the level of correlation in the channel, leading to lower usable spatial degrees of freedom. This leads to higher inter-user interference and in-turn a lower SINR is observed at the user terminal. Secondly, our proposed approximations are seen to remain sufficiently accurate for the entire SNR range for all cases. It is worth mentioning that in most statistical channel models, the *overall* geometric attenuation (combined effect of distance based attenuation with shadow fading) for a given terminal is *unrelated* to its K-factor. In practice, LoS links are known to leverage lower attenuation and less fading. In such cases, the resulting gains in the link budget may compensate for the loss of multi-path diversity. Moreover, the results presented here are for commonly considered scenarios, where the composite specular channel matrix may have a unit rank. It has been shown in [20] that for certain array geometries giving a full rank specular matrix, Ricean fading behaves like Rayleigh fading. Thus, it is likely that results for higher rank specular channels will be scenario dependent.

We now study the impact of increasing M on the expected per-user SINR with a fixed number of terminals in the system. Fig. 2 depicts the expected per-user SINR as a function of M with $L = 5$ at SNR $= 10$ dB. We observe that increasing M naturally increases the expected per-user SINR. However, the expected SINRs can be seen to slowly saturate with growing M. This is a result of channels to multiple terminals becoming asymptotically pairwise orthogonal, such that the inner product of any two channel vectors tends to zero. This has been famously coined as convergence to favorable propagation conditions in the large MIMO literature [21]. However, as we consider uncorrelated downlink transmission, the size of the ULA grows with the number of transmit antenna elements. Taking this into account, we only consider up to $M = 30$ transmit antennas with an inter-element spacing of a half wavelength. It can also be observed that an increase in the mean of K results in a slower growth in the expected per-user SINR. For all cases, the derived approximations remain tight and are robust to changes in system size. This is consistent with Remark 2.

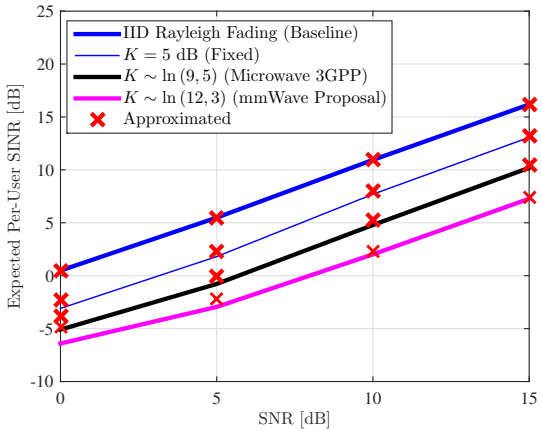

Fig. 1. Expected per-user SINR vs. SNR with $M = 10$ and $L = 3$.

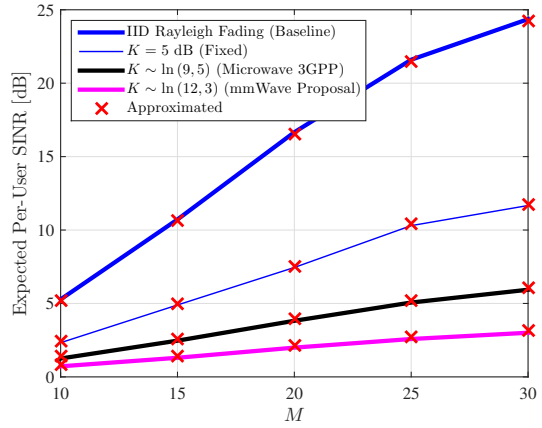

Fig. 2. Expected per-user SINR vs. M with $L = 5$ at SNR $= 10$ dB.

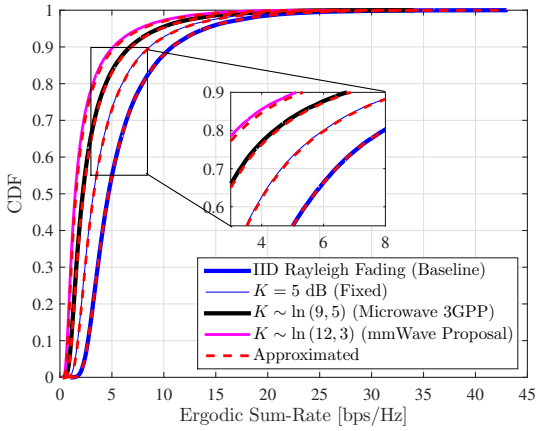

Fig. 3. Ergodic sum-rate CDFs with $M = 10$, $L = 3$ at SNR $= 10$ dB.

We now examine the influence of LoS on the ergodic sum-rate. Specifically, in Fig. 3 with $M = 10$ and $L = 3$ at SNR $= 10$ dB, we compare the cumulative distribution functions (CDFs) of the derived ergodic sum-rate approximation in (24) with its simulated counterpart. The ergodic sum-rate is obtained by averaging over fast-fading with the CDFs repre-

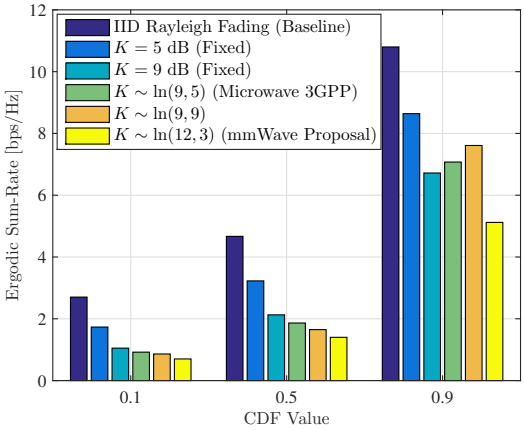

Fig. 4. Ergodic sum-rate comparison at CDF values of 0.1, 0.5 and 0.9 with $M = 10$, $L = 3$ at SNR $= 10$ dB.

senting the variations in the link gains and the K factors. We observe that although the approximations remain extremely tight, the sum-rates achieved from (24) are marginally higher than the simulated responses, due to the upper bound using Jensen's inequality. We again observe that a stronger specular component has an adverse effect on the ergodic sum-rate, which is seen to degrade with increasing K.

As a further matter, we investigate the impact of variability in K factors, for a constant mean. Fig. 4 depicts the ergodic sum-rate at the CDF values of 0.1, 0.5 and 0.9, respectively. We observe that increasing the variability of K at the CDF values of 0.1 and 0.5 leads to a degradation in the ergodic sum-rates. In contrast, at the upper end of the CDF (the peak rate scenario of CDF$=0.9$), increasing the variability improves the ergodic sum-rate. This behavior is related to the log-normal nature of the K factor distribution. Increasing the variance amplifies the range of K from zero to very large values. Hence, at the lower end of the sum-rate CDF, the increased occurrence of large K values tends to reduce performance. However, at the upper end of the CDF, where the sum-rate is already high, the increased variability helps as more K values close to zero are generated. Essentially, the increased variability in K increases the variability in the sum-rate and correspondingly the cell edge rates are lowered, while the peak rates are enhanced.

V. Conclusion

The paper presents a tight approximations of expected per-user SINR and achievable ergodic sum-rate of a MU-MIMO system with RZF precoding under Ricean fading channels. The analysis is robust to changes in system size, SNR levels and can be applied to LoS and NLoS channels. Arbitrary eigenvalue densities of the complex non-central Wishart channel correlation matrix are shown to be fundamental to the analysis. In deriving the expected SINR, we derive the joint density of two arbitrary eigenvalues for the non-central Wishart. Our results suggest that increasing the specular component of the channel has an adverse effect on the expected SINR and ergodic sum-rate, while increasing variability in the K factor enhances peak rates, while reducing cell-edge rates. To the best of the authors' knowledge, the evaluation of the variability of K is novel and can help to identify sensitivities in system performance.

Appendix A
Proof of Theorem 1

$$\mathbb{E}_\lambda\left[\sum_{i=1}^{m}\frac{(\lambda_i)^c}{(\lambda_i+\xi)^2}\right]=m\left[\int_0^\infty \frac{(\lambda)^c}{(\lambda+\xi)^2} f_0(\lambda)\, d\lambda\right], \quad (27)$$

where $f_0(\lambda)$ is the density of an arbitrary eigenvalue selected from $\{\lambda_1,\ldots,\lambda_m\}$. Using $f_0(\lambda)$ in [22] allows us to write (27) as

$$m\Bigg[\int_0^\infty \frac{(\lambda)^c}{(\lambda+\xi)^2}\frac{e^{-\sum_i \phi_i}}{m\left((n-m)!\right)^m}\frac{e^{-\lambda\left(\bar{K}+1\right)}}{\lambda}\sum_{j=1}^{m}\left(\left(\bar{K}+1\right)\lambda\right)^{n-m+j}$$

$$\sum_{\substack{i=1\\ i\neq j}}^{m}\sum_{p=0}^{\infty}\frac{\left(\left(\bar{K}+1\right)\phi_i\lambda\right)^p\mathcal{D}(i,j)}{p!\left(n-m+1\right)_p}\Bigg/\left(\prod_{k<q}^{m}\phi_q-\phi_k\right)d\lambda\Bigg]. \quad (28)$$

Extracting the constants and simplifying (28) yields

$$m\Bigg[\frac{e^{-\sum_i\phi_i}}{m\left((n-m)!\right)^m\prod_{k<q}^{m}\left(\phi_q-\phi_k\right)}\sum_{j=1}^{m}\sum_{\substack{i=1\\ i\neq j}}^{m}\sum_{p=0}^{\infty}\left(\bar{K}+1\right)^{n-m+j}$$

$$\frac{\left(\left(\bar{K}+1\right)\phi_i\right)^p\mathcal{D}(i,j)}{p!\left(n-m+1\right)_p}\int_0^\infty\frac{\lambda^{c-1+n-m+j+p}e^{-\lambda\left(\bar{K}+1\right)}}{\left(\lambda+\xi\right)^2}d\lambda\Bigg]. \quad (29)$$

We let $\bar{\mu}=c-1+n-m+j+p\geq 2$ and evaluate the integral in (29) via a change of variables, such that $\lambda=x-\xi$. This gives the integral in (29) as

$$\sum_{\gamma=0}^{\bar{\mu}}\binom{\bar{\mu}}{\gamma}(-\xi)^{\bar{\mu}-\gamma}e^{\xi\left(\bar{K}+1\right)}\int_\xi^\infty x^{\gamma-2}e^{-x\left(\bar{K}+1\right)}dx, \quad (30)$$

where the integral in (30) is as defined in (12). Substituting (30) into (29) and letting $\Theta=\frac{e^{-\sum_i\phi_i}}{m\left((n-m)!\right)^m\prod_{k<q}^{m}\left(\phi_q-\phi_k\right)}$ yields the desired expression in (10).

Appendix B
Proof of Theorem 2

Invoking Appendix A.2 of [22], the joint (unordered) density of the m eigenvalues, $\lambda_1,\ldots,\lambda_m$ of $\sqrt{\bar{K}}\bar{\boldsymbol{H}}+\boldsymbol{H}_w$ is given by

$$f\left(\lambda_1,\ldots,\lambda_m\right)=\Theta\prod_{k<q}^{m}\left(\lambda_k-\lambda_q\right)\prod_{k=1}^{m}\lambda_k^{n-m}e^{-\sum_{i=1}^{m}\lambda_i}\boldsymbol{\Xi}_1, \quad (31)$$

where $\boldsymbol{\Xi}_1$ is the determinant of ${}_0F_1\left(n-m+1,\phi_i\lambda_j\right)$, with ${}_0F_1(\cdot,\cdot)$ being the scalar hypergeometric function. Recognizing that ${}_0F_1(a,b)=(a-1)!b^{-(a-1)/2}\mathrm{I}_{a-1}\left(2\sqrt{b}\right)$, letting $\varsigma=n-m+1$ and decomposing the first product in (31) into a summation over permutations of $\{0,1,\ldots,m-1\}$, we can write (31) as

$$f(\lambda)=\Theta\left[(\varsigma-1)!\right]^m(-1)^{\left\lfloor\frac{m}{2}\right\rfloor}\sum_{\varrho}(-1)^{\mathrm{per}(\varrho)}\boldsymbol{\Xi}_2, \quad (32)$$

where $\boldsymbol{\Xi}_2$ is the determinant of $\phi_i^{-\frac{\varsigma-1}{2}}\lambda_j^{\frac{\varsigma-1}{2}+\varrho_j}e^{-\lambda_j}\mathrm{I}_{\varsigma-1}\left(2\sqrt{\phi_i\lambda_j}\right)$. To find $f(\lambda_1,\lambda_2)$, we integrate over $\lambda_3,\ldots,\lambda_m$, i.e., over columns $3,\ldots,m$ in $\boldsymbol{\Xi}_2$.

The resulting entries of $\mathbf{\Xi}_2$ can now be written as

$$\frac{\Gamma(\varsigma+\varrho_j)}{\Gamma(\varsigma)}\,{}_1F_1(\varsigma+\varrho_j,\varsigma,\phi_i). \tag{33}$$

Reordering the columns such that ϱ is ordered from $0,1,\ldots,m-1$ and performing the Laplace expansion on columns i,j (containing λ_1 and λ_2) yields

$$f(\lambda_1,\lambda_2)=\Theta\left[(\varsigma-1)!\right]^m(-1)^{\lfloor\frac{m}{2}\rfloor}(n-2)!\sum_{i=0}^{m-1}\sum_{\substack{j=0\\ j\neq i}}^{m-1}\sum_{r=1}^{m}\sum_{\substack{s=1\\ s\neq r}}^{m}$$
$$(-1)^u\,\mathbf{\Xi}(r,s;i,j)\,\phi_r^{-v/2}\lambda_1^{v/2+i}e^{-\lambda_1}\mathrm{I}_v\Big(2\sqrt{\phi_r\lambda_1}\Big)\,\phi_s^{-v/2}$$
$$\lambda_2^{v/2+j}e^{-\lambda_2}\mathrm{I}_v\Big(2\sqrt{\phi_s\lambda_2}\Big). \tag{34}$$

Further simplifying and denoting $u=i+j+r+s-p(i,j)-t(r,s)$, $v=n-m$, $C=\Theta\left[(\varsigma-1)!\right]^m(-1)^{\lfloor\frac{m}{2}\rfloor}(n-2)!$, $\tilde{\mathbf{\Xi}}(r,s;i,j)=(\phi_r\phi_s)^{-v/2}\,\mathbf{\Xi}(r,s;i,j)$ and $g_{a,b}(\lambda)=\lambda^{v/2+b}e^{-\lambda}\mathrm{I}_v\big(2\sqrt{\phi_a\lambda}\big)$ yields the expression in (13).

Appendix C
Proof of Theorem 3

Using the density derived in (13), we begin by stating

$$D_l=G_l^{(2)}+m(m-1)\int_0^\infty\int_0^\infty\left(\frac{\lambda_1}{\lambda_1+\xi}\right)\left(\frac{\lambda_2}{\lambda_2+\xi}\right)C\sum_{i=0}^{m-1}\sum_{\substack{j=0\\ j\neq i}}^{m-1}$$
$$\sum_{r=1}^{m}\sum_{\substack{s=1\\ s\neq r}}^{m}(-1)^u\,\tilde{\mathbf{\Xi}}(r,s;i,j)\,g_{r,i}(\lambda_1)\,g_{s,j}(\lambda_2)\,d\lambda_2 d\lambda_1, \tag{35}$$

where C, u and $g_{a,b}(\lambda)$ are as defined in (15) and (13), respectively. Substituting the definition of $g_{a,b}(\lambda)$ into (35) yields

$$D_l=G_l^{(2)}+m(m-1)\sum_{i=0}^{m-1}\sum_{\substack{j=0\\ j\neq i}}^{m-1}\sum_{r=1}^{m}\sum_{\substack{s=1\\ s\neq r}}^{m}(-1)^u\,\tilde{\mathbf{\Xi}}(r,s;i,j)J_{r,i}J_{s,j}, \tag{36}$$

for any two arbitrary eigenvalues (λ_1,λ_2), where

$$J_{a,b}=\int_0^\infty\frac{\lambda^{v/2+b+1}e^{-\lambda}\mathrm{I}_v\left(2\sqrt{\phi_a\lambda}\right)}{\lambda+\xi}d\lambda, \tag{37}$$

with $v=n-m$. To evaluate the above integral, we convert $\mathrm{I}_v\left(2\sqrt{\phi_a\lambda}\right)$ into its equivalent series form giving

$$J_{a,b}=\sum_{\varepsilon=0}^{\infty}\left[\frac{\phi_a^{\varepsilon+\frac{n-m}{2}}}{\varepsilon!\,(\varepsilon+n-m)!}\right]\int_0^\infty\frac{\lambda^{\varepsilon+n-m+b+1}e^{-\lambda}}{\lambda+\xi}d\lambda. \tag{38}$$

Denoting $\hat{\mu}=\varepsilon+n-m+b+1\geq 2$, we evaluate the integral in (38) with a change of variable, where $\lambda=x-\xi$. Upon doing this, after some simplifications we obtain

$$\int_0^\infty\frac{\lambda^{\hat{\mu}}e^{-\lambda}}{\lambda+\xi}d\lambda=\sum_{\gamma=0}^{\hat{\mu}}\binom{\hat{\mu}}{\gamma}(-\xi)^{\hat{\mu}-\gamma}\,e^{\xi}\int_\xi^\infty x^{\gamma-1}e^{-x}dx. \tag{39}$$

Note that the integral in (39) is a special case of the integral in (12). Substituting (39) into (38) and (38) into (36) yields the desired expression in Theorem 3.

References

[1] T. Marzetta, "Noncooperative cellular wireless with unlimited numbers of base station antennas," *IEEE Trans. Wireless Commun.*, vol. 9, no. 11, pp. 3590–3600, Nov. 2010.

[2] D. Gesbert, M. Shafi, D. Shiu, P. Smith, and A. Naguib, "From theory to practice: An overview of MIMO space-time coded wireless systems," *IEEE J. Sel. Areas Commun.*, vol. 21, no. 3, pp. 281–302, Apr. 2003.

[3] T. Yoo and A. Goldsmith, "On the optimality of multiantenna broadcast scheduling using zero-forcing beamforming," *IEEE J. Sel. Areas Commun.*, vol. 24, no. 3, pp. 528–541, Mar. 2006.

[4] C. B. Peel, B. M. Hochwald, and A. L. Swindlehurst, "A vector-perturbation technique for near-capacity multiantenna multiuser communication-Part I: Channel inversion and regularization," *IEEE Trans. Commun.*, vol. 53, no. 1, pp. 195–202, Jan. 2005.

[5] X. Gao, O. Edfors, F. Rusek, and F. Tufvesson, "Linear pre-coding performance in measured very-large MIMO channels," in *Proc. IEEE Veh. Technol. Conf. (VTC) Fall*, Sept. 2011, pp. 1–5.

[6] J. Hoydis, S. ten Brink, and M. Debbah, "Massive MIMO in the UL/DL of cellular networks: How many antennas do we need?" *IEEE J. Sel. Areas Commun.*, vol. 31, no. 2, pp. 160–171, Feb. 2013.

[7] S. Sun, T. Rappaport, R. Heath, A. Nix, and S. Rangan, "MIMO for millimeter-wave wireless communications: Beamforming, spatial multiplexing, or both?" *IEEE Commun. Mag.*, vol. 52, no. 12, pp. 110–121, Dec. 2014.

[8] Q. Zhang, J. Shi, K.-K. Wong, H. Zhu, and M. Matthaiou, "Power scaling of uplink massive MIMO systems with arbitrary-rank channel means," *IEEE J. Sel. Topics Signal Process.*, vol. 8, no. 5, pp. 966–981, Oct. 2014.

[9] C. Kong, C. Zhong, M. Matthaiou, and Z. Zhang, "Performance of downlink massive MIMO in Ricean fading channels with ZF precoder," in *Proc. IEEE Int. Conf. on Commun. (ICC)*, Jun. 2015, pp. 1776–1782.

[10] W. Tan, S. Jin, J. Wang, and M. Matthaiou, "Achievable sum-rate of multiuser massive MIMO downlink in Ricean fading channels," in *Proc. IEEE Int. Conf. on Commun. (ICC)*, Jun. 2015, pp. 1453–1458.

[11] D. Tse and P. Viswanath, *Fundamentals of Wireless Communication*. Cambridge University Press, 2005.

[12] F. Farrokhi, G. Foschini, A. Lozano, and R. Valenzuela, "Link-optimal space-time processing with multiple transmit and receive antennas," *IEEE Commun. Lett.*, vol. 5, no. 3, pp. 85–87, Mar. 2001.

[13] 3GPP TR 36.873 v.12.2.0, *Study on 3D channel models for LTE*. 3GPP, Jun. 2015.

[14] M. Akdeniz, Y. Liu, M. Samimi, S. Sun, S. Rangan, T. Rappaport, and E. Erkip, "Millimeter wave channel modeling and cellular capacity evaluation," *IEEE J. Sel. Areas Commun.*, vol. 32, no. 6, pp. 1164–1179, Jun. 2014.

[15] D. Nguyen and T.Le-Ngoc, "MMSE precoding for multiuser MISO downlink transmission with non-homogeneous user SNR conditions," *EURASIP J. Adv. Signal Process.*, vol. 85, no. 1, pp. 1–12, Jun. 2014.

[16] L. Yu, W. Yiu, and R. Langley, "SINR analysis of the subtraction-based SMI beamformer," *IEEE Trans. Signal Process.*, vol. 58, no. 11, pp. 5926–5932, Nov. 2010.

[17] H. Tataria, P. Smith, P. Dmochowski, and M. Shafi, "General analysis of multiuser MIMO systems with regularized zero-forcing precoding under spatially correlated Rayleigh fading channels," *in Proc. of IEEE Int. Conf. on Commun. (ICC)*, 2016.

[18] H. Tataria, P. Smith, M. Shafi, and P. Dmochowski, "Generalized analysis of coordinated regularized zero-forcing precoding: An application to two-tier small cell networks," *submitted to IEEE Trans. Wireless Commun.*, 2015.

[19] T. Thomas, H. Nugyen, G. MacCartney, and T. Rappaport, "3D mmWave channel model proposal," in *Proc. IEEE Conf. on Veh. Technol. (VTC-Fall)*, Sep. 2014, pp. 1–6.

[20] P. Driessen and G. Foschini, "On the capacity formula for multiple input-multiple output wireless channels: A geometric interpretation," *IEEE Trans. Commun.*, vol. 47, no. 2, pp. 173–176, Feb. 1999.

[21] E. Larsson, O. Edfors, F. Tufvesson, and T. Marzetta, "Massive MIMO for next generation wireless systems," *IEEE Commun. Mag.*, vol. 52, no. 2, pp. 186–195, Feb. 2014.

[22] G. Alfano, A. Lozano, A. Tulino, and S. Verdú, "Mutual information and eigenvalue distribution of MIMO Ricean channels," in *Proc. IEEE Int. Symp. Information Theory & Applications (ISITA)*, Oct. 2004.